A. F. H. Kaplan
Head of the Group
on European Projects
ISLT - Department
of Non-Conventional Processing,
Forming and Laser Technology,
Vienna University of Technology,
Arsenal, Objekt 207,
A-1030 Vienna, Austria

G. Groboth
Head of the Group on Materials Technology
Group on Materials Technology,
Austrian Research Center, Seibersdorf,
A-2444 Seibersdorf, Austria

Process Analysis of Laser Beam Cladding

The technology of laser beam cladding of metals by single-step powder delivery is analyzed with a process model which is based on balance equations of energy and mass. Effects like powder heating, clad layer formation, substrate dilution and overlapping of tracks are discussed in dependence of the process parameters. In particular, the powder catchment efficiency and the beam energy redistribution in the material can be optimized by the powder mass flow rate and by the geometrical properties of the beam and of the powder jet. [DOI: 10.1115/1.1344899]

Introduction

Surface processing of materials by high power laser beams [1] encompasses the technologies of laser hardening, laser remelting, laser glazing, laser alloying, laser dispersing, and laser cladding. Laser cladding of metal surfaces is integrated into industrial manufacturing lines in order to create surfaces with enhanced hardness, wear resistance, or corrosion resistance. Common industrial applications [2] cover cladding of gear shafts, cam-shafts, piston rings, extruder parts, engine exhaust valves [3], turbine blades, or pipes [4].

Laser cladding [1,5] is usually carried out by single-step powder delivery, illustrated in Fig. 1, i.e., during the laser heating process the powder is simultaneously blown to the workpiece surface rather than being preplaced in advance. The mechanism of the cladding process is as follows. The laser beam, focused for providing intensities in the order of 10^3-10^5 W/cm^2, is absorbed at the workpiece surface causing melt pool formation [6]. Simultaneously, the powder to be added is carried to the processing zone by a shielding gas jet through an inclined nozzle. The powder particles travel through the laser beam where they absorb a portion of the beam power. Those particles which enter the melt pool are molten in the pool and stick up during resolidification, thus forming a clad layer track due to continuous motion of the workpiece.

The substrate material, in most applications aluminum alloy or mild steel, shall usually be clad by a material of enhanced hardness. Common powders in use are Co- and Ni-base alloys and carbides [7,8] like the Co-base alloys Stellite 6 and Stellite F and the Ni-base alloy Deloro 50. Since melting of carbide powder is difficult and not desirable, a second powder component with lower melting point is added, thus providing a molten matrix for embedding the carbides. A typical composite coating consists of 60 percent WC/Co (88/12 mass percent) and 40 percent NiCrBSi, the latter acting as the matrix [9]. Besides the carbides TiC, SiC, or the ceramics ZrO_2 and $CrAl_2O_3$ are frequently used [10]. Moreover, stainless steel can be deposited in order to improve the corrosion resistance of unalloyed steel surfaces [11]. All materials mentioned above significantly increase the surface hardness and thus the wear resistance compared to technical surfaces of steel or aluminum.

Since the technology of laser beam cladding relies upon complex physical mechanisms, numerous experimental and theoretical investigations were conducted in the past in order to improve the understanding of the process. The experimental behavior of the cladding process was explained in simple equations by Weerasinghe and Steen [11]. Applying FE-methods, numerous researchers [12] have computed the thermocapillary Marangoni flow, induced by surface tension gradients, since it can significantly alter the melt pool shape. A model of laser cladding was elaborated by Picasso et al. [8] who demonstrated that absorption by the powder is proportional to the powder feeding rate. The model is not self-consistent, since it requires a prescribed clad layer height. Attenuation of the laser beam by the powder jet was also estimated by Li et al. [13]. Marsden et al. [7] and Pelletier et al. [14] discovered the significant geometrical influence of the areas of intersection between laser beam, melt pool and powder jet on the powder catchment efficiency. By stating a simple energy balance, Powell [15] estimated heating of the powder by the beam. Moreover, his experiments revealed that different shapes of cross sections can result, depending on the operating conditions. A model describing the diffusion effects during laser cladding was developed by Kar and Mazumder [16].

In general, optimization of the cladding process aims for maximum coverage rate, maximum powder catchment and beam absorption efficiency, but for minimum surface roughness and for strong clad layer adhesion, thus, improving the mechanical or the corrosion properties of the surface under optimum economic conditions.

The present work is based on a mathematical model that permits theoretical analysis of the laser cladding process, which enables the derivation of useful optimization strategies for process parameters in industrial applications.

Mathematical Model

Energy Balance. Heating of the powder and of the bulk material is considered by stating energy balances. According to Fig. 1, two mechanisms of powder heating can be distinguished: (1) heating of the powder during traveling through the laser beam, (2) subsequent heating by the melt pool. The two mechanisms are discussed by Kaplan et al. [17,18] in more detail.

Heating of a powder particle by the laser beam can be calculated by the following energy balance [17,18]:

$$h_p(t)=c_pT_a+\frac{3r_p^2\pi}{\rho 4r_p^3\pi}\frac{1}{\nu_p\cos\beta}\alpha_p\int_{-\infty}^{x_p(t)}I(x,y)dx-\Delta h_r \quad (1)$$

where h_p is the average specific enthalpy of the powder particle. Δh_r can take into account the heat of formation of additional chemical reactions (negative for exothermic reactions). Real powder particles are irregular in shape, while in the model they are approached by equivolumetric spheres with an average powder particle radius r_p. The powder absorption coefficient α_p is averaged over the angle of incidence according to the grain surface. While traveling through the laser beam along a trajectory $x_p(t)$

Contributed by the Manufacturing Engineering Division for publication in the JOURNAL OF MANUFACTURING SCIENCE AND ENGINEERING. Manuscript received April 1998; revised April 2000. Associate Editor: S. G. Kapoor.

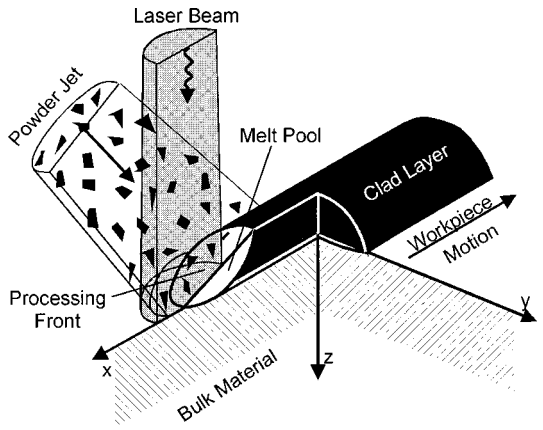

Fig. 1 Basic mechanism of single-step laser beam cladding

$=x_{p0}+tv_p\cos\beta$ (at fixed y-coordinate) each powder particle is heated by the absorbed beam intensity $\alpha_p I(x_p(t),y)$ that has to be integrated along the trajectory ($dt=dx/v_p\cos\beta$) and multiplied by the particle interaction cross section $r_p^2\pi$ in order to obtain the rise of enthalpy of the powder. Here the powder injection angle β is defined relative to the workpiece surface. As proven by numerical estimations, heat losses of the powder particle by radiation and convection can be neglected. Moreover, the spatial enthalpy distribution in the particle approaches equilibrium in a short time scale (0.01–0.1 ms) compared to the dwelling time (1 ms). From the enthalpy h_p the average temperature T_p of the powder particles can be derived by an enthalpy transformation that takes into account latent heat of melting Δh_m:

$$\begin{aligned} h_p<h_s: T_p&=\frac{h_p}{c_p}\\ h_s\leqslant h_p<h_l: T_p&=T_m\\ h_l\leqslant h_p: T_p&=\frac{h_p-\Delta h_m}{c_p}\end{aligned} \tag{2}$$

where

$$h_s=c_pT_m$$

$$h_l=c_pT_m+\Delta h_m$$

are the solidus and liquidus enthalpies, respectively. Any chemical reactions can be correspondingly considered by their temperature and enthalpy of phase change.

The temperature field $T(x,y,z)$ in the bulk material is calculated by the model of a moving Gaussian source of heat scanning over a semi-infinite workpiece surface [19]:

$$T(x,y,z)=T_a+\frac{\alpha P_L}{Kr_b}\int_0^\infty\frac{\exp(-H)}{(2\pi^3)^{1/2}(1+\mu^2)}d\mu \tag{3}$$

with the function

$$H(\mu)=\frac{(X+\mu^2R/2)^2+Y^2}{2(1+\mu^2)}+\frac{Z^2}{2\mu^2}$$

α is the surface absorption, already considering attenuation by the powder jet [8]. Equation (3) has been extended [20] by superimposing different Gaussian beams in order to approach real, non-Gaussian beam intensity distributions. The above approach is very useful, because the whole temperature field can easily be calculated by an analytical expression. However, applied to laser cladding Eq. (3) contains several strong simplifications. Latent heat of melting is neglected. Theoretical studies have shown that this simplification shifts the isotherms, but their size remains similar, in particular since latent heat of melting and resolidification compensate each other in the overall energy balance, but they of course appear at different locations. An enthalpy transformation can be applied in order to consider latent heat. As in most analytical solutions, thermal conductivity is taken independent of temperature [21]. By proper choice of an average value the error in the calculation remains little, as investigated earlier. In the present study the thermal properties are averaged over the solid range, thus from ambient to melting temperature. Therefore any temperature gradients are overestimated in regions of high conductivity and underestimated in domains of low conductivity, which slightly alters the shape of the melt pool. Moreover, Eq. (3) can only be applied to a homogeneous substrate with a flat surface. Thus the geometry of the clad layer as well as the different thermal conductivity are not considered. This strong simplification was necessary in order to apply an analytical solution. It can be justified by the fact that heat conduction is mainly governed by the large bulk material compared to the confined clad layer. The model assumes that the dimensions of the melt pool in the clad layer will be of similar size than for the case of a flat surface. Surface heat losses due to radiation and convection are neglected, an often applied simplification for modeling of laser materials processing, justified by several authors. In addition, thermocapillary melt flow due to Marangoni convection, which can widen the melt pool, is not considered in the model in order to keep it simple.

From Eq. (3) the boundary of the liquid pool, described by its characteristic dimensions of maximum length $l_m(y)$ and depth $d_m(y)$ as a function of y, and the average pool temperature T_{mp}, or enthalpy h_{mp} by adding the latent heat of melting, can be calculated.

When the powder particle enters the liquid pool, it contains an initial enthalpy h_{pl} which results from heating by the beam, Eq. (1). The particle is surrounded by melt at average enthalpy h_{mp}, yielded from Eq. (3), corresponding to an instationary boundary value problem of Dirichlet type with prescribed enthalpy at the surface of a sphere. An analytical solution of this problem [21] is:

$$h_p(r,t)=h_{p1}+\frac{r_p(h_{mp}-h_{p1})}{r}\sum_{n=0}^{\infty}\left[\operatorname{erfc}\left(\frac{(2n+1)r_p-r}{2\sqrt{\kappa t}}\right)-\operatorname{erfc}\left(\frac{(2n+1)r_p+r}{2\sqrt{\kappa t}}\right)\right]-\Delta h_r$$

The powder enthalpy, spatially averaged over the spherical particle coordinate r [17,18], is

$$h_p(t)=h_{p1}+(h_{mp}-h_{p1})\frac{3\sqrt{\kappa t}}{r_p}\left[\frac{2}{\sqrt{\pi}}-\frac{\sqrt{\kappa t}}{r_p}+4\sum_{n=1}^{\infty}i\operatorname{erfc}\left(\frac{nr_p}{\sqrt{\kappa t}}\right)\right]-\Delta h_r \tag{4}$$

Again, the enthalpy transformation Eq. (2) is applied for deriving the corresponding powder temperature T_p from h_p. Chemical reactions can be considered when calculating the powder heating cycle, Eq. (1), Eq. (4), because these equations yield the enthalpy and in the subsequent enthalpy transformation, Eq. (2), any heat of formation can be considered.

In order to estimate the maximum clad layer cross section A_c a theoretical upper energy limit can be stated. This approach, which is not part of the model but serves for claiming a theoretical physical limit, is valid for high cladding rates, assuming that all absorbed laser power is solely consumed for melting the clad layer. An energy efficiency coefficient η_e can be stated:

$$\eta_e=\frac{\nu A_c\rho(h_l-c_pT_a)}{\alpha P_L}=\frac{\nu A_c\rho[c_p(T_m-T_a)+\Delta h_m]}{\alpha P_L}\leqslant 1 \tag{5}$$

Mass Balance. The mass balance relates the mass flow rate of the striking powder to the workpiece motion, consequently yielding the clad layer height d_c (see Fig. 2(*b*)):

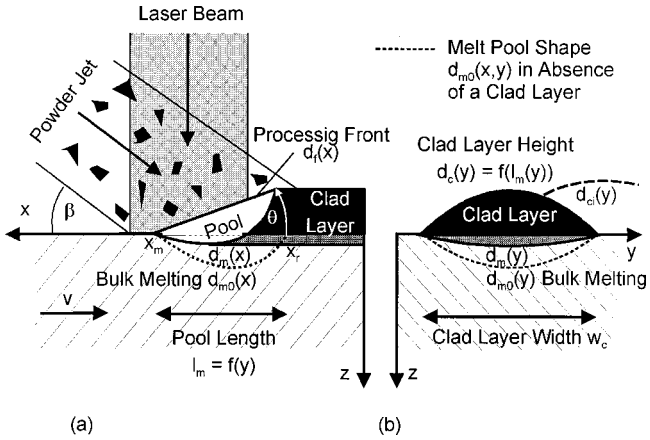

Fig. 2 Model geometry: (*a*) side view, (*b*) cross section

$$d_c(y)\,v = \eta_p \frac{l_m(y)}{\tan\beta}\frac{\dot{m}_p}{\rho r_j^2 \pi}$$

$$d_c(y) = \eta_p \frac{1}{\rho r_j^2 \pi \tan\beta}\frac{l_m(y)\dot{m}_p}{v} \tag{6}$$

The clad layer height is proportional to the length of the melt pool $l_m(y)$ resulting from Eq. (3) and to the ratio between the powder mass flow rate $\dot{m}_p$ and the processing speed v. Consequently, the angle of inclination θ of the processing front results from the mass balance Eq. (6):

$$\tan\theta \equiv \frac{d_c(y)}{l_m(y)} = \eta_p \frac{1}{\rho r_j^2 \pi \tan\beta}\frac{\dot{m}_p}{v} \tag{7}$$

Geometry. The model relies on the assumption that the dimensions of the melt pool during laser cladding remain similar compared to pure surface melting in the absence of a clad layer. The process geometry is thus defined by the melt pool dimensions (see Fig. 2) which in turn determine the clad layer cross section $d_c(y)$. At the surface, the melt pool interface solid-liquid can be described by the melting front $x_m(y)$ and by the resolidification front $x_r(y)$ which in turn determine the length of the melt pool $l_m(y) = x_r(y) - x_m(y)$ required for $d_c(y)$, Eq. (6). The cross section $d_{m0}(y)$ of the melt pool determines the remolten bulk material in absence of powder. When a clad layer $d_c(y)$ forms, Eq. (6), the clad powder linearly sticks on the melt pool from the front to the rear, thus yielding the processing front angle θ, Eq. (7) (see Fig. 2(*a*)) and creates the front surface $d_f(x,y) = (x - x_m(y))\tan\theta$. Assuming that the relative depth $d_{m0}(x,y)$ of the melt pool remains unchanged, while the surface $d_f(x,y)$ has been elevated, the absolute values of the molten bulk cross section are also elevated to a maximum depth $d_m(y) = \min_x\{d_f(x,y) - d_{m0}(x,y)\}$.

Dilution η_d is defined as the ratio of molten bulk material of cross section A_b to the total molten cross section $A_c + A_b$:

$$\eta_d = \frac{A_b}{A_c + A_b} \tag{8}$$

Moreover, the geometry of the powder jet has to be taken into account, which is projected onto the workpiece surface leading to an elliptical area according to its diameter and angle of incidence (see also Fig. 1 and Fig. 2(*a*)). If this ellipsis does not cover the entire processing front, a smaller, effective powder-covered melt pool length $l_m^*(y)$ has to be considered in Eq. (6) by geometrically cutting off the calculated melt pool surface $x_f(y), x_r(y)$ point-by-point at the borders of the impinging powder jet.

The shape $d_c(y)$ that is obtained point-by-point from Eq. (6) can be approximated by a potential law function

$$d_c(y) = d_{c0}\left(1 - \left(\frac{2y}{w_c}\right)^p\right) \tag{9}$$

where d_{c0} is the central clad layer height, w_c is the clad layer width and the exponent p is obtained from a calculated intermediate point, e.g., by inserting $y = w_c/4$ into Eq. (6). The shape $d_c(y)$ results from the mass balance, while fluid flow and surface tension effects are not considered in order to keep the model simple.

Consideration of surface tension is a difficult task that needs additional comprehensive investigation due to the complexity of the surface geometry (see Fig. 1), the interaction with the impinging powder particles, and the dependence of the surface tension on temperature and impurities, which also causes Marangoni flow. As a first order approach surface tension forces, $\sigma/r = 650 - 1600\ \mathrm{N/m^2}$, dominate against gravity, $\rho g d_c = 40 - 150\ \mathrm{N/m^2}$, by one order of magnitude (here: iron) for typical geometries of laser cladding. Thus, minimizing the surface area causes a circular cross section of the track that is approached by a parabolic shape in the model, Eq. (9), which is very similar and easier to solve. Neglecting surface tension effects causes an error in the shape of the track cross section, thus in track height and width. The error increases with increasing powder feeding rate because larger cross sections cause smaller radii of the surface curvature and in turn dominating forces. Comparison with experimental results of Powell [15] and Weerasinghe and Steen [11] yields very similar shapes (error <5 percent) at low powder feeding rate and geometrical deviations of 10–30 percent for high powder delivery. For very high powder feeding rates the track approaches a drop-like cross section wider than the melt pool that cannot be described by Eq. (9), but by a circle of equivalent cross section. An approach similar to Eq. (9) can be stated for the bulk melt cross section $d_m(y)$. From these approximations, the area of the cross sections A_c and A_b can be calculated analytically by integration, e.g., for the clad layer:

$$A_c = \int_{-w_c/2}^{+w_c/2} d_c(y)\,dy = d_{c0} w_c \left(1 - \frac{1}{p+1}\right) \tag{10}$$

For overlapping tracks the basic cladding mechanism remains similar, which means that the width and the area of the track remain unchanged. The shape $d_{c,i}(y)$ of the new clad sticks onto the shape $d_{c,i-1}(y - \Delta y_b)$ of the previous clad according to the track displacement Δy_b. Since a smooth curved shape can be expected the potential law Eq. (9) is again applied to obtain the new shape $d_{c,i}(y)$. The shape is achieved by tilting the original cross section $d_c(y)$, however, under consideration of conservation of mass, i.e., of A_c.

Results and Analysis

The numerical investigations focus on laser cladding of Stellite 6-powder (Co-base-alloy, 28 percent Cr, 4 percent W, 1 percent C; grain size $2r_p = 50\,\mu\mathrm{m}$) blown ($\beta = 30°$, $2r_j = 3$ mm, $\eta_p = 80$ percent) on a mild steel substrate by a cw-CO_2-laser beam with flattened intensity profile [20]. Powder heating is shown in Fig. 3 for particles that enter the pool at three different locations x_e: close to the melting front x_m, close to the resolidification front x_r and at an intermediate location $x_e = x_m + 0.5$ mm. Observation of an individual powder particle shows that it initially is heated when flying through the laser beam (1: beam heating), and then it enters the pool at a location determined by the flight trajectory of the particle. In the pool the particle is heated by the surrounding melt pool (2: pool heating) until it is in thermal equilibrium with the melt pool (3: equilibrium) and subsequently experiences the same heating and quenching cycle as the melt pool. Although powder melting takes place in the demonstrated case of high beam focusing, usually heating by the laser beam merely enhances the temperature but does not normally cause melting, as also concluded by Pustovalov and Bobuchenko [22]. Once the

particles enter the melt pool, they are molten within a few microseconds, which is a negligible duration compared to the traveling time l_m/v through the pool. The mechanism of pool heating is determined by the pool temperature. Therefore carbides like WC-powder are not molten due to the much higher melting point. Co and stainless steel have similar melting points below unalloyed steel; consequently they are molten by a steel pool, but also by their own pools since the pool temperature exceeds the melting point, which is considered in the calculation, too. The specific material aspects for blown powder are discussed in more detail by Kaplan et al. [17,18]. Reaching equilibrium with the pool, powder and substrate undergo the same quenching cycle, except for the resolidification transition.

The clad layer height and width decrease with increasing processing speed, as shown in Fig. 4. Comparisons with experimental data from Weerasinghe and Steen [11] are in good agreement with the calculations. The decrease in width can be explained by narrowing of the melt pool, while the decrease in height is caused by the reduced number of powder particles per unit length due to the higher speed. Despite the strong simplification of the model, predictions of the clad layer cross sections also were in good agreement with experimental shapes obtained by Weerasinghe and Steen [11] and Powell [15].

For moderate mass flow rates, the clad layer height is proportional to the powder feeding rate, since it is limited by the mass balance, Eq. (6), as illustrated in Fig. 5. However, for large clad layer cross sections the fundamental energy limit, Eq. (5), is reached. Any additional powder cannot melt and is thus lost, as also observed experimentally [15,23]. The most efficient operating point is achieved at the mass flow rate that corresponds to the point of intersection of both limits, which means that, both, powder and energy losses are minimized. Moreover, the influence of speed and power can be seen in Fig. 5, both shifting the limits. The corresponding dilution is plotted in Fig. 6 as a function of the powder feeding rate. The melting depth and in turn the dilution drops from 100 percent for absence of powder to 0 percent at moderate powder rates which means that severe dilution can be easily avoided when applying sufficiently high powder feeding rates, leading to an optimum operation range. Thus the remelted track of the substrate diminishes for thick clad layers and dilution vanishes. Beyond this limit the substrate is solely liquid at the leading front $x_m(y)$ which is thus responsible for adhesion between the clad layer and the substrate while the whole melt pool is completely shifted into the clad layer. Moreover, the higher the clad layer height the better the energy efficiency η_e, Eq. (5). In the energy-limited range, i.e., for $\eta_e = \alpha_p$, no additional clad growth can take place, while in turn powder efficiency decreases with increasing mass flow rate.

Overlapping tracks for two different degrees of overlap are shown in Fig. 7. Larger overlap increases the final clad layer

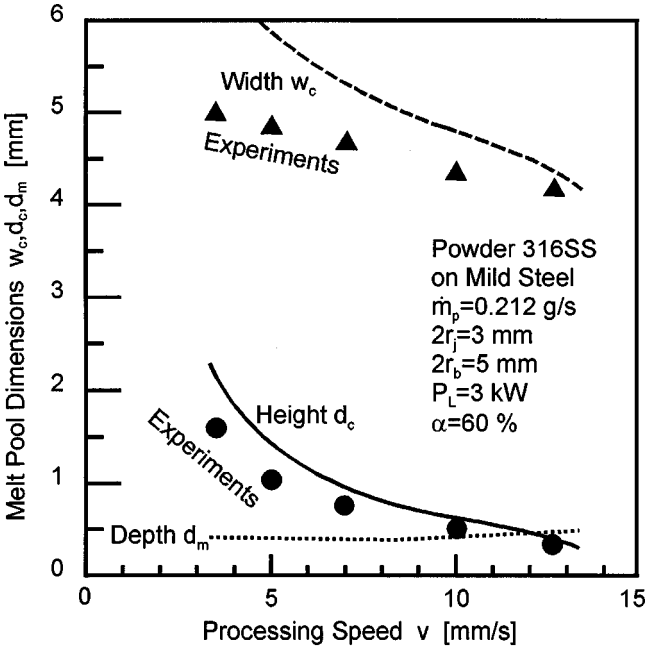

Fig. 4 Experimental (Weerasinghe and Steen, 1987) and calculated melt pool and clad layer dimensions in dependence of the processing speed for laser cladding of stainless steel on mild steel

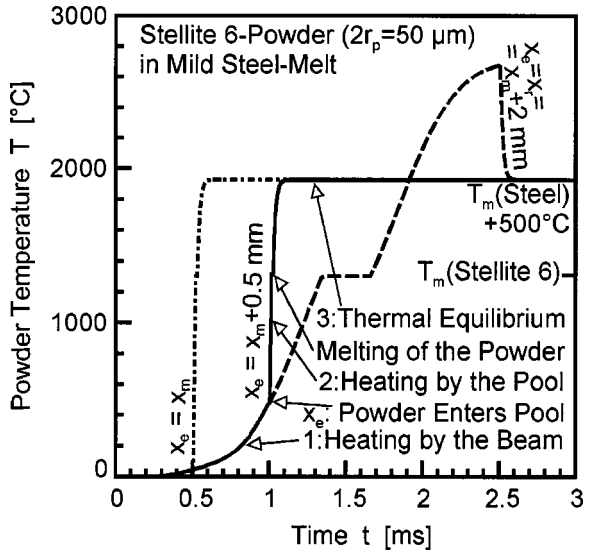

Fig. 3 Heating of a Stellite 6-powder particle as a function of time; (1) heating by the laser beam, (2) heating by the melt pool, (3) equilibrium with the melt pool; the three curves correspond to particles with different pool entrance location x_e

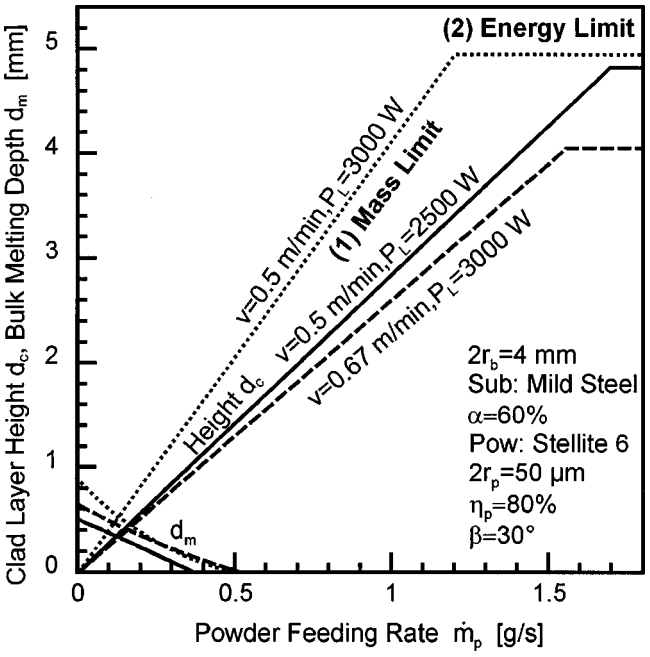

Fig. 5 Clad layer height and bulk melting depth as a function of the powder feeding rate for varying translation speed and beam power; height limited by: (1) mass balance, (2) energy balance

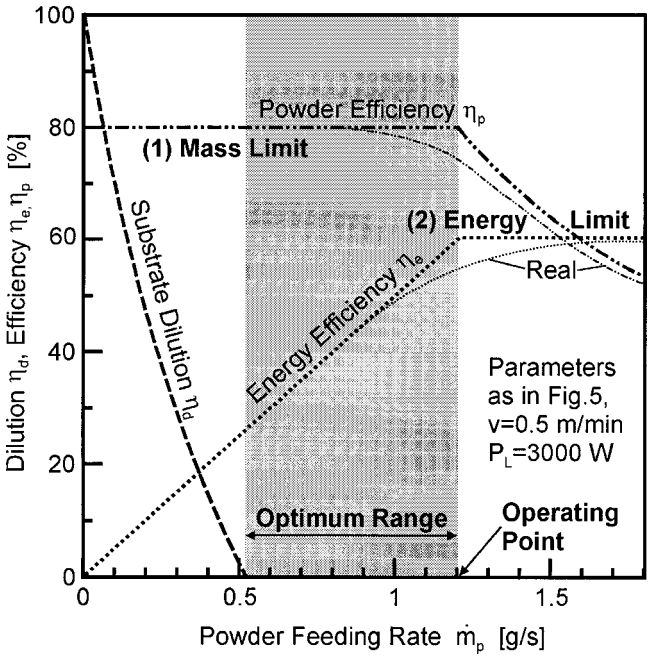

Fig. 6 Substrate dilution, powder catchment and powder heating efficiency as a function of the powder feeding rate, corresponding to Fig. 5

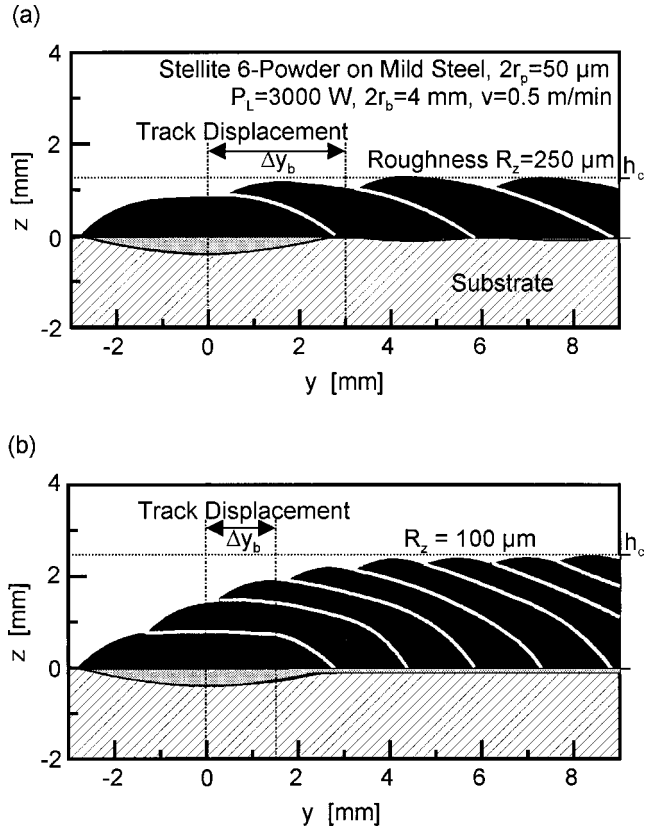

Fig. 7 Cross sections of overlapping clad layer tracks: (*a*) little overlap (45 percent, Δy_b=3 mm), (*b*) significant overlap (75 percent, Δy_b=1.5 mm)

height and decreases the surface roughness R_z. A few tracks are necessary for reaching a constant state of overlapping tracks. Dilution shifts from the bulk material in case of a single track to the previous clad layer during overlapping.

The applicability of the model to real processes fails for high intensities if vaporization occurs. Moreover, pulsed processing cannot be considered in the present model. Real surface conditions can be considered in the absorption coefficient and real intensity distributions can be modeled [20].

Conclusions

(i) An analytical model of laser beam cladding has been elaborated based on balances of mass and energy, accompanied by geometrical aspects.

(ii) The model permits calculation of the temperature distribution in the workpiece, of powder heating, and of the resulting clad layer shape.

(iii) The powder is heated (1) by the beam (relatively slow, 1 ms), (2) by the pool (almost immediately, 10 μs), (3) by equilibrium quenching (slow, 10–100 ms).

(iv) Beam melting has to be avoided, which is easily possible for moderate beam focusing.

(v) The stacking limits for the clad height are governed by the balances of either mass or energy and by the borders of the powder jet.

(vi) In order to avoid bulk dilution, the mass flow rate and the processing speed have to exceed a lower limit.

(vii) However, vanishing dilution causes worse layer adherence, since only the leading curve of the processing front is then responsible for resolidification.

(viii) Large overlap causes low clad surface roughness and high layer thickness.

Acknowledgments

The authors are grateful to Professor D. Schuöcker for enabling this work, that was funded by the Austrian National Science Foundation (FWF), grant no. P11384-ÖPY.

Nomenclature

A_b = bulk melting cross section, m^2
A_c = clad layer cross section, m^2
c_p = specific heat capacity, $Jkg^{-1}K^{-1}$
d_c = clad layer height, m
d_{c0} = central clad layer height, m
d_m = substrate melting depth, m
d_{m0} = d_m in the absence of powder, m
$d_{c,i}$ = height of clad layer i, m
erfc( ) = complementary error function,
$h_l = h_s + \Delta h_m$ = liquidus enthalpy, Jkg^{-1}
h_p = enthalpy, powder particle, Jkg^{-1}
h_{p1} = enthalpy, powder after beam heating, Jkg^{-1}
$h_s = c_p T_m$ = solidus enthalpy, Jkg^{-1}
h_{mp} = melt pool enthalpy, Jkg^{-1}
$H( )$ = function, see Eq. (3)
i = index of overlapping tracks
ierfc( ) = integral of complementary error function
$I(x,y)$ = beam intensity distribution, Wm^{-2}
K = thermal conductivity, substrate, $Wm^{-1}K^{-1}$
l_m = melt pool length, m
$\dot{m}_p$ = mass flow rate, powder, kgs^{-1}
p = exponent, cross section
P_L = laser beam power, W
r = radial co-ordinate, powder, m
r_b = laser beam radius, m
r_j = powder jet radius, m
r_p = radius powder particle, m
$R = r/r_b$ = dimensionless beam radius
t = time, s
T = temperature, K
T_a = ambient temperature, K
T_m = melting temperature, K
T_{mp} = average melt pool temperature, K
T_p = powder temperature, K

v = processing speed, ms^{-1}
v_p = powder particle velocity, ms^{-1}
w_c = clad layer width, m
x = coordinate, parallel, m
x_m = melting front location, m
x_e = entrance powder into pool, m
x_p = powder flight location, m
x_r = resolidification front, m
$X=x/r_b$ = dimensionless coordinate
y = coordinate, lateral, m
$Y=y/r_b$ = dimensionless coordinate
z = coordinate, vertical, m
$Z=z/r_b$ = dimensionless coordinate
α = absorption, surface
α_p = absorption, powder
β = powder jet angle, rad
Δh_m = latent heat of melting, Jkg^{-1}
Δh_r = heat of formation of chemical reactions, Jkg^{-1}
Δy_b = track displacement, m
η_d = dilution
η_e = energy efficiency
η_p = powder catchment rate
κ = thermal diffusivity, ms^{-2}
θ = processing front angle, rad
ρ = specific density, powder, kgm^{-3}
μ = dimensionless time $\mu=\sqrt{2\kappa t}/r_b$

References

[1] Steen, W. M., 1986, ''Laser Cladding, Alloying and Melting,'' *The Industrial Laser Annual Handbook*, D. Belforte and M. Levitt eds., pp. 158–174.
[2] Gebhardt, A., Kreutz, E. W., and Backes, G., 1996, ''Reconditioning of Machine and Engine Parts using High-Power Lasers,'' *Proceedings, ECLAT'96*, Stuttgart (D), **1**, pp. 373–381.
[3] Küpper, F., Gasser, A., Kreutz, E. W., and Wissenbach, K., 1990, ''Cladding of Valves with CO_2 Laser Radiation,'' *Proceedings, ECLAT'90*, Erlangen (D), pp. 461–467.
[4] Hatakenaka, H., and Yamadera, M., 1995, ''Development and Application of Preventive Maintenance Technique for Pipes Using Laser Cladding Method,'' Karyoku-Genshiryoku-Hatsuden, **46**, No. 9, pp. 950–956.
[5] Yellup, J. M., 1995, ''Laser Cladding using the Powder Blowing Technique,'' Surf. Coat. Technol., **71**, pp. 121–128.
[6] Tosto, S., 1994, ''Laser Surface Treatments: A Review of Models,'' Lasers Eng., **3**, pp. 157–186.
[7] Marsden, C. F., Hoadley, A. F. A., and Wagnière, J.-D., 1992, ''Characterization of the Laser Cladding Process,'' *Proceedings, ECLAT'92*, Erlangen (D), pp. 543–551.
[8] Picasso, M., Marsden, C. F., Wagnière, J.-D., Frenk, A., and Rappaz, M., 1994, ''A Simple but Realistic Model for Laser Cladding,'' Metall. Trans. B, **25B**, pp. 281–291.
[9] Grünenwald, B., Shen, J., Dausinger, F., and Nowotny, St., 1992, ''Laser Cladding with a Heterogeneous Powder Mixture of WC/Co and NiCrBSi,'' *Proceedings, ECLAT'92*, Erlangen (D), pp. 411–418.
[10] Pei, Y. T., Ouyang, J. H., and Lei, T. C., 1996, ''Microstructure of Bonding Zones in Laser-Clad Ni-Alloy-Based Composite Coatings Reinforced with Various Ceramic Powders,'' Metall. Mater. Trans. A, **27**, No. 2, pp. 391–400.
[11] Weerasinghe, V. M., and Steen, W. M., 1987, ''Laser Cladding with Blown Powder,'' Met. Constr., No. 10, pp. 581–585.
[12] Thompson, M. E., and Szekely, J., 1989, ''The Transient Behavior of Weldpools with a Deformed Free Surface,'' Int. J. Heat Mass Transf., **32**, pp. 1007–1019.
[13] Li, W. B., Engström, H., Powell, J., Tan, Z., and Magnusson, C., 1995, ''Modelling of the Laser Cladding Process: Pre-Heating of the Blown Powder Material,'' Lasers Eng., **4**, pp. 329–341.
[14] Pelletier, J. M., Sahour, M. C., Pilloz, M., and Vannes, A. B., 1993, ''Influence of Processing Conditions on Geometrical Features of Laser Claddings Obtained by Powder Injection,'' J. Mater. Sci., **28**, pp. 5184–5188.
[15] Powell, J., 1983, *Laser Cladding*, Ph.D thesis, Imperial College of Science and Technology, Dept. of Metallurgy, London (UK).
[16] Kar, A., and Mazumder, J., 1987, ''One-Dimensional Diffusion Model for Extended Solid Solution in Laser Cladding,'' J. Appl. Phys., **61**, pp. 2645–2655.
[17] Kaplan, A. F. H., Weinberger, B., and Schuöcker, D., 1997, ''Theoretical Analysis of Laser Cladding and Alloying,'' *SPIE Proceedings, LASER'97-Lasers in Material Processing*, Munich (D), **3097**, pp. 499–506.
[18] Kaplan, A. F. H., Liedl, G., Zimmermann, J., and Spruzina, W., 1998, ''Laser Dispersing of TiC-Powder into Al-Substrates,'' Lasers Eng., **7**, Nos. 3–4, pp. 165–178.
[19] Cline, H. E., and Anthony, T. R., 1977, ''Heat Treating and Melting Material with a Scanning Laser or Electron Beam,'' J. Appl. Phys., **48**, pp. 3895–3900.
[20] Kaplan, A. F. H., 1997, ''Surface Processing with Non-Gaussian Beams,'' Appl. Phys. Lett., **70**, pp. 264–266.
[21] Carslaw, H. S., and Jaeger, J. C., 1959, *Conduction of Heat in Solids*, 2nd ed., Oxford Univ. Press, New York.
[22] Pustovalov, V. K., and Bobuchenko, D. S., 1993, ''Thermal Processes in Gas-Powder Laser Cladding of Metal Materials,'' Int. J. Heat Mass Transf., **36**, pp. 2449–2456.
[23] Jouvard, J.-M., Grevey, D. F., and Lemoine, F., 1997, ''Continuous Wave Nd:YAG Laser Cladding Modeling: A Physical Study of Track Creation During Low Power Processing,'' J. Laser Appl., **9**, pp. 43–50.